International Journal of Information Technology and Applications
Volume 1, Issue 3, September 2024 ISSN 3007-7397 © P-Learn Press

Benchmarking Single Image Dedusting

Yang Chen[1], Xinxin Xu[2], Chuansheng Wang[3], Fuquan Zhang[4*]

[1] *Fujian Key Laboratory of Automotive Electronics and Electric Driving Technology, Fujian University of Technology*
[2] *New Engineering Industry College, Putian University, China*
[3] *Polytechnic University of Catalonia, Spain*
[4]*College of Computer and Control Engineering, Minjiang University, China*

chenyang515@qq.com, XxinXu04@163.com, wangcs95@163.com, zfq@mju.edu.cn

Abstract. Dusty image enhancement has been attracted wide attention due to its practicability in autonomous and monitoring systems. However, little methods focus on advanced learning-based dedusting models due to the difficulty of collecting paired training data. To bridge this problem, this paper proposes a new large-scale benchmark dataset synthetized by the proposed synthetic method, named Realistic Single Image Dust Removal (RSIDR), for image dedusting task, which consisting both synthetic and corresponding real-world dusty images. In addition, we present a comprehensive study and evaluation for the state-of-the-art image enhancement methods on image dedusting task. We further provide a large variety of criteria metrics for image evaluation, ranging from full-reference Image Quality Assessment (IQA) to no-reference IQA. Experiments on RSIDR reveal the limitations and advantages of the existing image enhancement algorithms, and suggest promising research directions.

Keywords: Dedusting, Synthetic dataset, Evaluations, Fourth keyword.

1. Introduction

1.1. Problem Description: Single Image Dedusting

Images captured from outdoor scenes often suffer from low brightness, poor visibility and color shift due to the dust in the air, which badly affect the scene visibility for people, and the performance of the traditional object recognition methods [1, 2, 3]. Recently, image dehazing task has attracted wide attention [4, 5, 6], however, few researchers pay attention to image dedusting as equal important image processing task. Different from other aerosols (e.g., haze, mist and fog), the existence of dust adds yellowing, nonlinear, depth-dependent noise to the outdoor images, and thus makes the image dust removal (a.k.a. dedusting) a highly difficult image enhancement and restoration problem [7, 8, 9]. Moreover, the presence of dust also affects the performance of many computer vision algorithms (e.g., image segmentation [10, 11, 12, 3], signal processing [13, 14], and image Generation [15]). Therefore, dedusting has becoming an increasingly worthy image pre-processing for both pattern recognition and image segmentation, whose research will immediately benefit many application [16, 17, 18].

Early researches considered the image dehazing is an important image restoration task, and made a huge contribution on this ffeld. Atmospheric scattering model can be used to describe the reason for degradation of

imaging results captured from detection system, and has been used in the classical description for natural scene generation:

$$I(x) = J(x)t(x) + A(1 - t(x)) \tag{1}$$

where $I(x)$ is the captured images, $J(x)$ is the recovered images. Eq. (1) has two critical parameters: A is the global atmospheric light, and $t(x)$ denotes the transmission matrix, which can be defined as:

$$t(x) = e^{-\beta d(x)} \tag{2}$$

where $d(x)$ is the depth between the object and camera, "*/beta*" is the scattering coefficient. Most state-of-the-art single image dehazing methods exploit the physical model and estimate the key parameter A and $t(x)$. Need to noted, Eq. (1) and Eq. (2) can also be the theoretical basis of the dusty image synthesis in this paper.

1.2. Dusty Image Synthetic Method

Similar with fog, the influences degree of images damaged by dust is also depend on the depth of scene. However, there have a huge different in physical property between dust and other aerosols (e.g., fog, mist and haze). Therefore, the relationship of depth maps between clear images and dusty images should be complied statistics by a rational method.

Dust-code: Dusty images and the corresponding clear images are essential component to quantitative compile statistic the degree of damage from dust in depth-depended. Collecting the paired images is difficult in any ill-posed image processing tasks. Therefore, recovering the clear images from real-world dusty images is a feasible method to collect paired images. DRHNet [5] is an excellent CNN-based image enhancement algorithm, which achieves the state-of-the-art performance both in image dehazing and deraining task. The generalization ability of DRHNet has been prove by the large amount of experiments both in synthetic and real-world datasets. Therefore, we preliminarily conduct image dedusting by DRHNet, and then using Photoshop to refine the dedusted results. Those operation can obtain the paired images in dusty and clear condition.

According to Eq. (1) and Eq. (2), depth information is the key to recover the clear scenes from the bad weather images and vice versa. Monocular depth estimation algorithm can assess the depth information just by single image. As far as we know, the monodepth2 [19] has achieve the state-of-the-art performance in monocular depth estimation of dusty and refined clear images, which is the key to compile statistics the relationship of the depth information between dusty and clear images. The relationship between dusty and its corresponding clear images can be named as dust-code. To estimate the dust code accurately, we collected twenty real-world dusty images from the Internet and previous papers.

Dust-code can be understood as the influence of dust working on depth estimation result obtained by monocular depth estimation algorithm. Figure 1 gives the flowchart of the dust code's estimation. After obtaining the dust-code, we can obtain a synthetic dusty image directly by following expression:

$$I(x) = J(x)\big(1 - p(x)d(x)\big) + C(p(x)d(x)) \tag{3}$$

where, $I(x)$ is the synthesized dusty images, $J(x)$ is the captured clear images, $p(x)$ denotes the proposed dust-code, and $d(x)$ is the image depth map evaluated by Monodepth2 [19].

1.3. Our contribution

Despite the practicability of single image dedusting algorithm, there still have following hurdles to the further development of this ffeld: ffrst, there is a lack of largescale public dataset. Second, current related image processing algorithms just focus on image dehazing and deraining, which seriously affected the advance of image dedusting. Third, current IQA for evaluating image enhancement algorithms are mostly just full-reference metrics, which is insufffcient for evaluating either human perception quality or machine vision effectiveness.

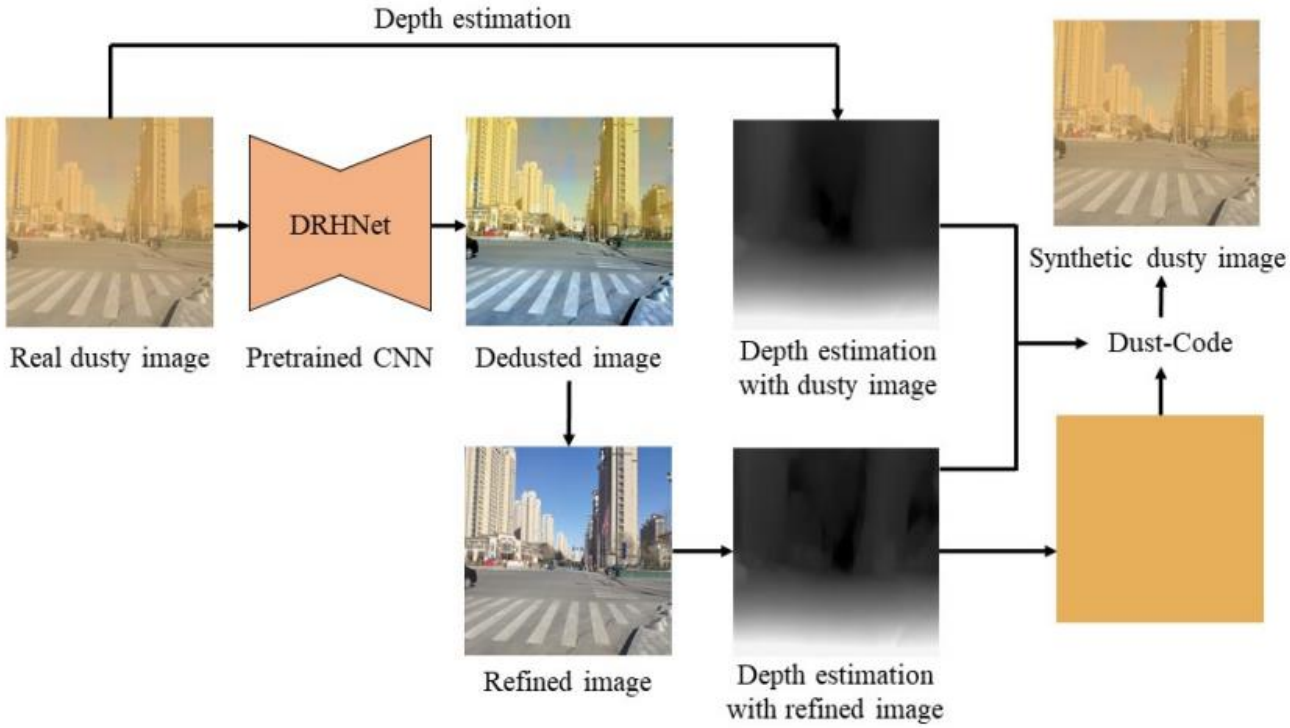

Figure 1. Synthetic method of dusty images.

Figure 1. Synthetic method of dusty images. The flows of synthetic method form left to right. Given a real-world dusty image to pretrained CNN for preliminary dedusting. The refined operations by Photoshop on preliminary dedusted images. Monodepth2 was be used to estimate the image depth information of the original dusty image and the refined images, then dust-code can be obtained. We can synthesize the dusty images from a clear image by the obtained dust-code.

The motivation of this paper is to directly overcome above problems, and makes the following three-fold contributions:

- We propose a novel and reasonable method to synthesize dusty images by giving clear images, which will bloom he development of image dedusting field. The proposed method fully considers the characteristics of the real dust images, including color, depth, brightness and other physical characteristics. Part of the synthetic dusty images are shown in Figure 1.
- We introduce a new single image dust removal dataset, called the Realistic single image dust removal (RSIDR). As far as we know, this is the first public available image dedusting dataset. The proposed dataset includes 9381 synthetic street scene dusty images, 4347 synthetic indoor dusty images, 20 hybrid synthetic dusty images, and 10 real-world dusty images. Among them, the published dataset includes training set, verification set and test set, respectively. A large number of datasets can ensure that our published dataset can meet the learning-based image

dedusting algorithms.

- We conduct an extensive range of experiments to conduct quantitative and qualitative comparison on six state-of-the-art image enhancement algorithms by running on RSIDR dataset. Moreover, we evaluate and analyze the advantage and limitation of each compared algorithms, and elaborate rich insights. The presented summarize and statement can point out the right direction to researchers who engaged in image dedusting research.

An overview of RSIDR could be found in Table 1. The RSIDR is the first and only systematic evaluation, that includes a number of image enhancement algorithms with multiple criteria on the proposed large-scale dataset. The RSIDR dataset is made publicly available for research purposes, and we plan to periodically update our own benchmarking results for noticeable new dedusting algorithms. We also welcome authors to report new results on RSIDR.

2. The Proposed Large-Scale Dataset: RSIDR

The proposed Realistic Single Image Dust Removal (RSIDR) is the first large-scale dataset for fairly evaluating the performance in image dedusting algorithms. A prominent feature of RISDR is the adequate experiments and the diversity of its evaluation criterion, ranging from traditional full-reference metrics, no-reference metrics, and even task driven evaluation. The performance of the state-of-the-art image enhancement algorithms in image dedusting will be discussed later in this paper.

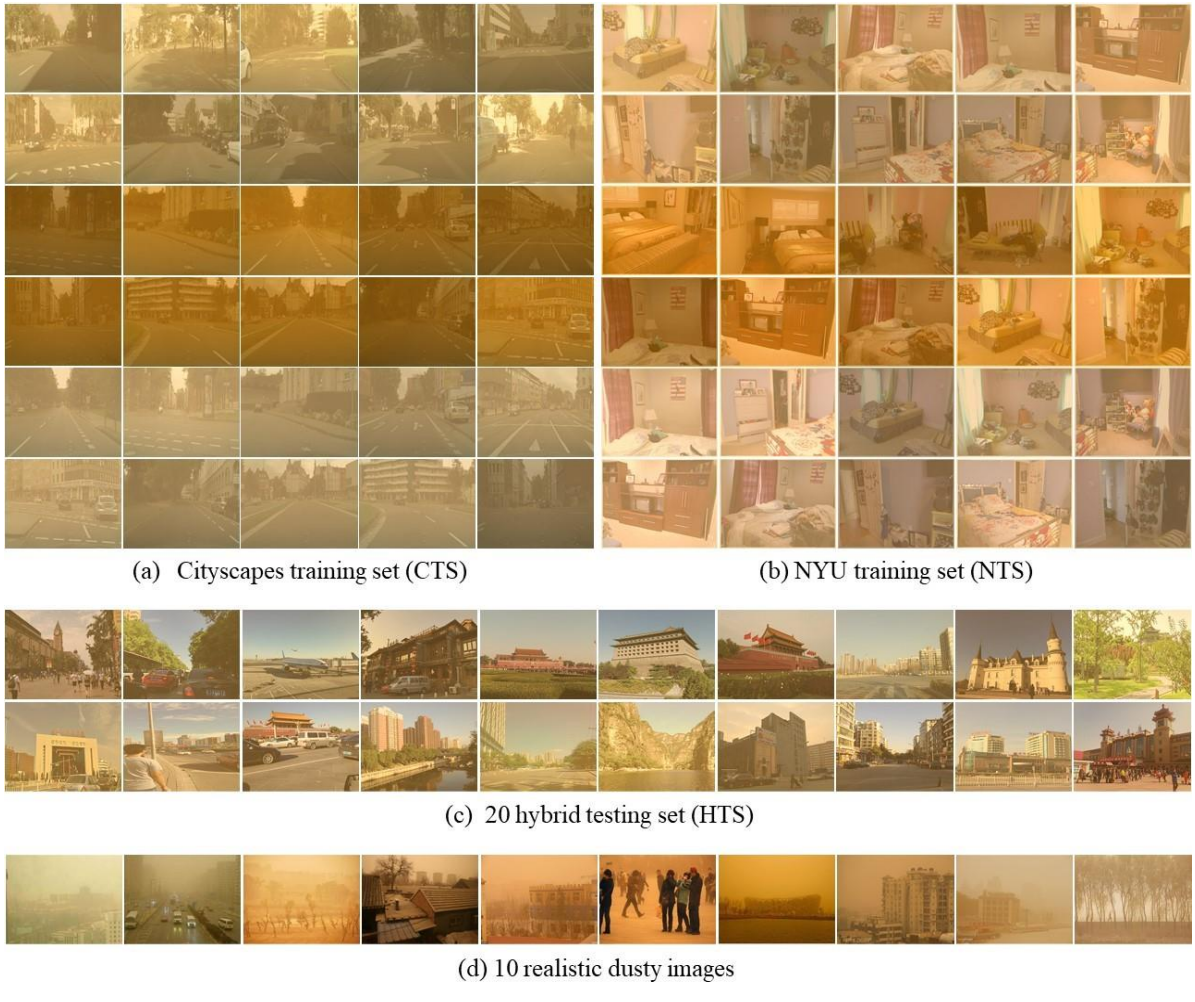

Figure 2. Example images from the four sets in RSIDR.

Table 1. Structure of RSIDR.

RSIDR(Cityscapes)			
Subest	*Number of Images*	*real/synthetic*	*Indoor/outdoor*
Street Training Set(STS)	8580	synthetic	outdoor
Street Validation set(SVS)	801	synthetic	outdoor
RSIDR(NYU)			
Subest	*Number of Images*	*real/synthetic*	*Indoor/outdoor*
Indoor Training Set(ITS)	3000	synthetic	indoor
Indoor Validation set(IVS)	1347	synthetic	indoor
RSIDR(Hybrid)			
Subest	*Number of Images*	*real/synthetic*	*Indoor/outdoor*
Hybrid Training Set(HTS)	20	synthetic	outdoor
RSIDR(Real-world images)			
Subest	*Number of Images*	*real/synthetic*	*Indoor/outdoor*
Real-world images	10	real	outdoor

2.1. Related Datasets

With the development of computer vision, more image datasets have been presented to developed to various pattern recognition task. For comprehensive consideration, both outdoor and indoor scenes need to be considered. Urban street scenes and indoor scenes are important of image dehazing, which have been used to synthesize outdoor and indoor hazy images. Therefore, there scenes are also important in image dedusting task.

(1) Cityscapes: Urban street scenes have attracted wide attention due to its practicability. The visual complexity of such scenes poses a serious challenge to the state-of-the-art computer vision algorithms. Cityscapes dataset [20], which can be used for urban streetscape understanding and automatic driving. Cityscapes consists of street scene video clips collected from 50 cities, whose training set, verification set and test set are including 2975, 500 and 1525 video clips respectively. Each video clip has 30 frames, and only the 20th frame is labeled at the pixel level for sematic segmentation. Franke et al. improved the basic Cityscapes dataset as authoritative databases in semantic segmentation, instance-wise and dense pixel annotations. The Cityscapes synthesis researchers adopt it to conduct other important computer vision tasks.

(2) NYU: Nathan Silberman et al. presented a dataset, which contains 1449 RGBD images to advance the 3D interpretation related researches. The main interest of Nathan et al. is to better understand how 3D cues can best inform a structured 3D interpretation. Therefore, Nathan Silberman et al. Offered a new dataset of 1449 RGBD images, capturing 464 diverse indoor scenes, Nathan Silberman et al. presented NYU depth dataset for 3D scene analysis, depth estimation and other computer vision tasks. Recently, some researchers adopted NYU-depth dataset for image dehazing.

(3) Dataset overview: Through the observation and statistics of a certain number of real dusty images captured by monitoring or cinema, combined with the characteristics of the images taken in the dust weather, we get three most common dusty colors, and the colors of dust storm as shown in Figure 3. Moreover, we set random number

between [0.8, 1.2] to adjust brightness randomly.

The RSIDR training set contains 13,728 synthetic dusty images, generated using 4,576 clear images from existing outdoor dataset Cityscape [20] and indoor depth dataset NYU [21]. We synthesize 3 dusty images for each clear image. An optional split of 11,580 for training and 2,148 for validation is provided. More specifically, 8,580 synthetic dusty images in the training set are synthesized by Cityscapes, and 3,000 synthetic dusty images are synthesized by NYU dataset. In validation set, 801 images are synthesized from Cityscapes, and 1,347 indoor dusty images are synthesized from NYU dataset. An overview of RSIDR could be found in Table 1.

2.2. Evaluation Strategies

It is inevitable to mix some interference factors to images (e. g. noise, blur, data loss) in the processing of image acquisition and display, which will cause the degradation of image quality (degradation, distortion). The quality of image has a direct impact on people's subjective feelings and information acquisition. Recently, the question of image quality evaluation has been widely. Image quality evaluation can be divided into subjective evaluation method and objective evaluation method. The subjective evaluation is conducted by the observer. Generally, the subjective score or the different mean opinion score are used. However, subjective evaluation work is time-consuming and inconvenient, so little researchers have studied it carefully. Objective evaluation method is to calculate the image quality index by computer according to a certain algorithm. According to whether reference image is needed in evaluation, it can be divided into three kinds of evaluation methods: full-reference, reduced-reference and no-reference. In the evaluation of distorted image, the full reference methods need to provide an undistorted original image, which is often difficult to get in practical application. The reduced-reference methods do not need to compare the distorted image with the original image, but only need to compare part features of the distorted image with the original image. No-reference image quality evaluation methods according to the self-characteristics of the distorted image without reference image. Although no reference method has the most practical value, it is more difficult to evaluate the quality of the image because there is not reference image, and the contents of the image are different. Different kinds of image quality objective evaluation strategies are shown in the Figure 8.

(1) Full-reference strategies: Peak Signal to Noise Ratio (PSNR) is a classical full-reference image evaluation metric to evaluate the performance of the image enhancement algorithms, which can be described as follow:

$$PSNR = 10log_{10}\frac{(2^n-1)^2}{MSE} \tag{4}$$

(2) No-reference strategies: Despite the popular of the full reference PSNR/SSIM metrics for evaluation dedusting algorithms, they are inherently limited due to the unavailability of clean ground truth images in practice, as well as they often poor alignment with human perception quality. Therefore, we refer to two no-reference IQA metrics: spatial-spectral entropy-based quality (SSEQ) [22], and Image Entropy, to complement the shortness of full-reference strategies. The score of SSEQ used in are range from 0 to 100, and the smaller the score the better the image quality. However, in order to make correlation consistent to full-reference metrics, we reverse the SSEQ score in this paper. For image entropy metric, the higher image entropy value means more details and changes in the image brightness. On the contrary, the image with lower entropy value has less image color details.

We will apply both full-reference (PSNR and SSIM) and no-reference (SSEQ and Image Entropy) evaluation

metrices to evaluate the dedusted results on synthetic images, and use SSEQ and Image Entropy on real-world images. We also will further compare those objective measures with subjective ratings.

Figure 3. The different colors obtained by the statistics of different real-world dusty images are used to synthesize different dusty images.

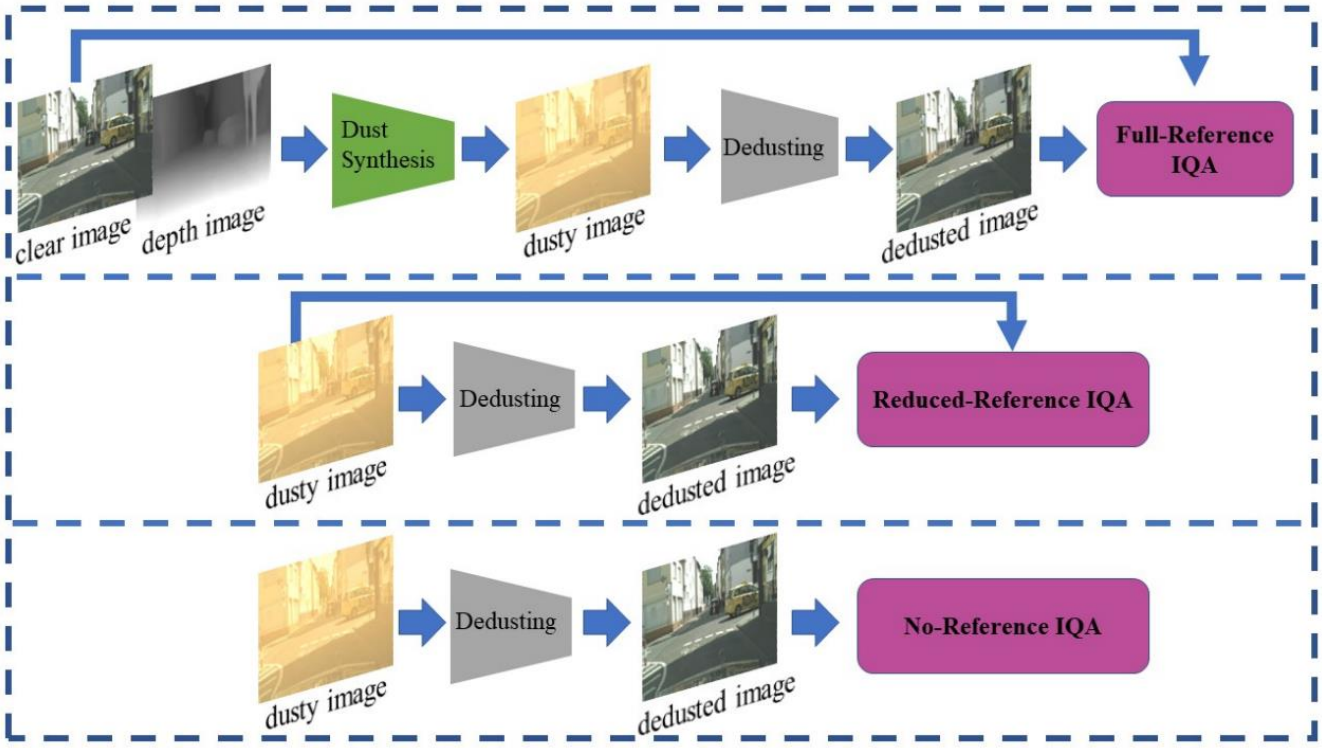

Figure 4. Three kinds of image quality objective evaluation methods.

3. Experimental Results

Based on the rich resources provided by RSIDR, we evaluate 6 representative state-of-the-art related image

enhancement algorithms: Double Deep-Image-Priors (DoubleDIP) [23], Allin-One Dehazing Network (AOD-Net) [24], Lightweight Pyramid Networks (LPNet) [25], Residual Guide Network (RGNet) [26], Feature Fusion Attention Network (FFANet) [27], and DedustNet proposed by our other work. DoubleDIP is a latest comprehensive computer vision method, which can be used to tackle a variety of seemingly unrelated tasks, such as image segmentation, layer separation image dehazing. AODNet is a typical CNN-based image dehazing method. LPNet and RGNet are the state-of-the-art image deraining methods. FFANet is the excellent learning-based model, which is based on feature fusion attention module. And DedustNet is designed for single image dedusting. In particular, the training epochs of all above data-driven methods are set to 200, and the size of training images are resized to 256*512 in the specify training process. Due to these methods are similar to image dedusting methods to some extent, they can be used to perform image dedusting task. The synthetic datasets and the model trained by these datasets all be present in https://github.com/jiayanHuang/RSIDR.

3.1. Results on Synthetic Datasets

In order to obtain different synthetic dusty images, we use three different dusty color maps as input for the proposed dusty images synthetic method, where the color maps are approximately hypothesized according to common dusty scenes in real-world. Therefore, we got the corresponding three different synthetic dusty datasets based on Cityscapes and NYU respectively, and produce three models trained by different synthetic dusty images generated by three different colors. Furthermore, we will mix the tree different synthetic dusty image datasets as training of networks to obtain a mix color model suitable for different real-world dusty scenes, and then use it to test on HTS and real-world images. For the evaluation of dedusting results, the average peak signal-tonoise ratio (PSNR) and structural similarity (SSIM) between the recovered images and the ground truths are used as the quantitative evaluation indexes. We first compare the dedusted results on STS and ITS using two full-reference (PSNR, SSIM) and two no-reference metric (SSEQ, Image Entropy). Table. III displays the detailed scores of each algorithm in terms of each metric. We can observe from Table. III that the DedustNet generates dedusted results with highest PSNR, and SSIM values than those of other algorithms results on both STS and ITS. The average PSNR and SSIM values of the DedustNet on STS dedusted results are 21.84 and 0.2916 higher than those of input dusty images, and on ITS dedusted results are 18.39 and 0.1808 higher than those of input dusty images, which demonstrates that the DedustNet is able to remove dust storm and generates high-quality images. FFANet [27] obtains the suboptimal PSNR value and third SSIM value on STS. AODNet [24] and RGNet [26] achieve the similar PSNR and SSIM values on STS. However, for ITS, AODNet gets a lower PSNR value, and RGNet obtains suboptimal PSNR and SSIM values.

When it comes to no-reference metrics, the results become less consistent. DedustNet still maintains competitive performance by obtaining the best SSEQ score and suboptimal Image Entropy score results on STS, and further illustrates highest Image Entropy score on ITS, thanks to the learning ability of its end-to-end network. DoubleDIP [23] ranks first in term of Image Entropy on STS. On the other hand, AODNet, LPNet, RGNet and FFANet get lower Image Entropy values than the original dusty images on STS. This may be due
to color distortion during their recovery process. For ITS, FFANet gets highest SSEQ score, and RGNet get suboptimal performance in terms of SSEQ and Image Entropy.

We show two examples of dedusting results from STS and ITS in Figure 4. From the comparison of the experimental results of several recent image enhancement-based methods on the RSIDR, we can find that the

DedustNet can produce more visually pleasant dedusted results on both STS and ITS. AODNet and FFANet can remove dust storm on outdoor scenes in some extant. However, the dedusted results on indoor images, the colors of restored images obtained by RGNet and FFANet are seriously changed, and thus make the dedusted results look unnatural. The DoubleDIP is committed to improving the brightness of images, and ignored the recovery of the dusty color. The RGNet make the colors of outdoor dedusted results become deeper. LPNet can reduce a certain degree of dust storms, however, there are deeper shadows on the edges of its all recovered images.

We have further conducted an experiment on HTS, whose dusty images have more details and color changes. Similarly, Table. 3 show quantitative evaluation results on our synthetic hybrid testing dataset (i.e. HTS) in terms of both full-reference and no-reference metrics. As seen from Table 3, DedustNet obtains highest PSNR value, SSEQ and Image Entropy score, which illustrates its effectiveness in image dedusting task. RGNet achieves second higher in terms of PSNR, SSIM and SSEQ. AODNet shows its highest SSIM value compared with other methods.

For qualitative evaluation of dedusted results on HTS, Figure 5 illustrates eight dedusted examples obtained by 6 state-ofthe-art methods. And we can observe that, the dedusted results obtained by DoubleDIP are becoming bright, but the colors of dedusted results are leaded to deeper at same times. AODNet gets obvious dedusting effect. LPNet and RGNet make the colors of final restored images distortion, and thus look unnatural. FFANet gets more bright effect dedusted results, such as the images of (f) from Figure 5. And the DedustNet can obviously remove dust storms from images, but the color saturations of restored results are degraded compared with the ground truths.

3.2. Results on Real-world Datasets

Although we train all six networks on synthesized dusty images, it can also be generalized to real-world dusty images. Figure 6 shows eight dusty images in real scenes and the corresponding dedusted results generated by several state-ofthe-art image enhancement-based algorithms. For DoubleDIP [29], the dust storms are barely removed or even become more sever visually in some cases, as observed in the second image of (b) in Figure 6. AODNet [30], and FFANet [33] can reduce a certain degree of dust storms for certain images, such as the first mage and the last two images. However, the effects of the two methods are worse when they are applied to the images with many details and deep colors, as observed in the third images and the five images of (c) and (f), respectively. Although LPNet [31] and RGNet [32] have certain effect of dedusting, they sometimes cause image color distortion, and thus make the recovered images seem unnatural, such as the last two images of (d), and the second, third and fourth images of (e). As shown in the last column of Figure 6, DedustNet achieves obvious effectiveness of image dedusting, and protects the image details in large degree as well, such as the windows of buildings in the sixth image, and the dense leaves of trees in the last image.

For quantitatively evaluation for real-world dedusted results, we adopt two no-reference metrics as the evaluation indexes. Table 3 illustrates average no-reference evaluation results of dedusted results on real-world images. Form Table 3, we observe that our DedustNet achieves the highest SSEQ and Image Entropy scores, which means that the method shows its obvious superiority in image dedusting task compared with other five methods. Notice again, we reverse the SSEQ score to make the correlation consistent to full-reference metrics.

According to the observation, the RGB histogram of a clean weather image is basically coincident and evenly distributed in the value space. In contrast, from Figure 7, we can find that the RGB color distribution of a real-world dusty image is relatively separate, and concentrated in a certain value range. Figure 7 shows two examples

of RGB histogram of dedusted results obtained by different methods. As Figure 7 shows, for the first example, which contains multiple clear objects, DoubleDIP and AODNet make the color distribution interval larger in certain degree. The RGB color distributions of LPNet, RGNet and FFANet become relatively coincident. And DedustNet not only makes the color distribution basically coincide, but also distributes evenly in the whole color value space, which meaning the dedusted results obtained by DedustNet are more effectiveness. For the second example, that contains more image detail, such leaves of tree, DoubleDIP makes the RGB distribution over the entire range generally, but the RGB color distributions is still basically not coincident, which is directly reflected in its visual subjective feeling. AODNet, LPNet, RGNet and FFANet make the distribution of three colors relatively concentrated and coincide, but all of them are still limited to a certain range. DedustNet shows its effectiveness in processing dusty image with more details.

Besides, in order to observe restored image detail information of dedusted real-world results more intuitively, we further extract image edges from the dedusted images obtained by different methods based on Canny Operator, respectively. Figure 8 illustrates texture maps of three different common scenes (including city, person and vehicle). From Figure 8, we can find that all of the six image-enhancement-based methods can preserve the image edge details in different degrees. Specifically, for city scene, all the compared methods have obvious effect on the restoration of the edge detail of close-up scenery, such as the building in first row images of Figure 8. In addition, FFANet and DedustNet can further recover some detail of remote objects. For person scene, as shown in the third and fourth row of Figure 8, all compared methods restored a large number character details, which are very useful for the following high-level computer vision tasks, such as target detection, automatic driving recognition technology. And as illustrated in the last two rows of Figure 8, for the vehicle scene, almost all methods can make vehicle details clear, and DedustNet can restore part of the road scene details.

3.3. Running Times

Table 5 reports the single image running time of each algorithm, averaged over the street scene images (256 * 512) in RSIDR, using a machine with 1.80 GHz CPU and 8G RAM. All methods are implemented in Python. AODNet is the most efficiency method thanks to its light weight structure. And the DedustNet costs second short running time on HTS, which is showing the second higher image dedusting speed.

4. Conclusion

In recent years, dusty weather is becoming more and more frequent. The occurrence of dust storm not only effects the visibility of the scene, but also may affect the driving safety. However, the real-world dusty image dataset is small and difficult to collect, which hinders the related research in the field of image dedusting. Therefore, in this paper, we propose a large-scale synthetic dusty image dataset, named RSIDR, which is the first systematic and published dusty image dataset to promote the further development of this field. In addition, we systematically evaluate 6 the-state-of-art image enhancement-based methods in single image dedusting task on the proposed RSIDR. For the evaluation of dedusted results obtain by different methods, rather than solely use full reference metrices, such as PSNR/SSIM, which need dusty clean image pair as input, we further conduct no-reference metrices (including SSEQ and Image Entropy) to evaluate the restored results of both synthetic and real-world dedusted results, so as to quantitatively evaluate 6 different algorithms more comprehensively.

Acknowledgment

The authors would like to thank Dr. David Root and Dr. Jean-Pierre Teyssier at Agilent Technologies for the loan of the time-domain nonlinear measurement equipment and TriQuint Semiconductor for the donation of the transistors.

Table 2. Average full-reference and no-reference evaluations results of dehazed results on STS and ITS.

STS							
Methods	Inputs	DoubleDIP [29]	AODNet [30]	LPNet [31]	RGNet [32]	FFANet [33]	DedusNet
PSNR	13.09	14.24	20.48	17.70	21.60	22.42	34.93
SSIM	0.6835	0.7413	0.8443	0.7939	0.8753	0.8651	0.9751
SSEQ	74.52	61.38	83.28	75.27	73.03	69.00	85.59
Entropy	6.62	7.44	6.26	6.57	5.95	6.51	6.75
ITS							
PSNR	14.69	13.70	16.94	15.75	21.62	15.09	33.08
SSIM	0.7534	0.7701	0.8071	0.7947	0.8764	0.7483	0.9342
SSEQ	63.59	56.97	63.29	49.03	64.47	65.07	56.67
Entropy	7.29	7.15	6.92	7.02	7.44	7.16	7.73

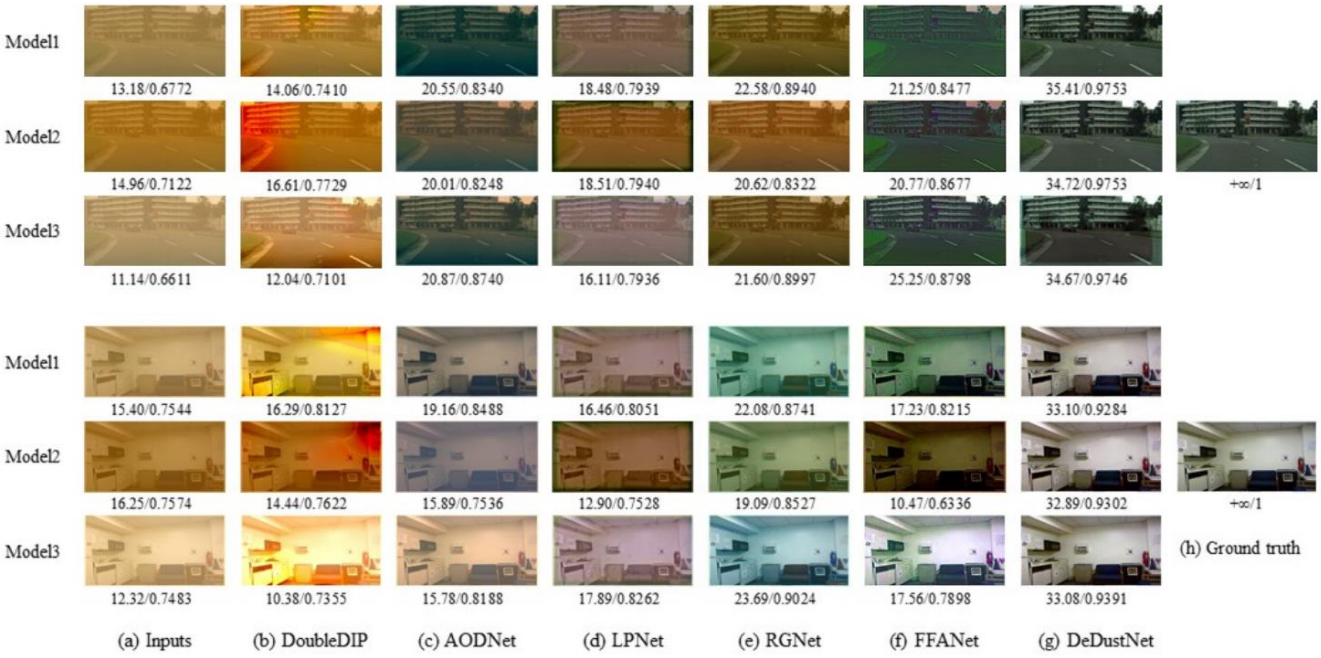

Figure 5. Examples of dedusted results on synthetic dusty images from CTS and ITS respectively.

Table 3. Average full-reference and no-reference evaluations results of dehazed results on STS and ITS.

Methods	DoubleDIP [29]	AODNet [30]	LPNet [31]	RGNet [32]	FFANet [33]	DedustNet
PSNR	16.97	19.64	19.20	21.03	14.92	21.25
SSIM	0.8129	0.8999	0.8678	0.8765	0.5477	0.8764
SSEQ	73.68	80.45	78.42	80.74	79.75	80.94
Entropy	7.48	7.13	7.35	7.15	7.18	7.68

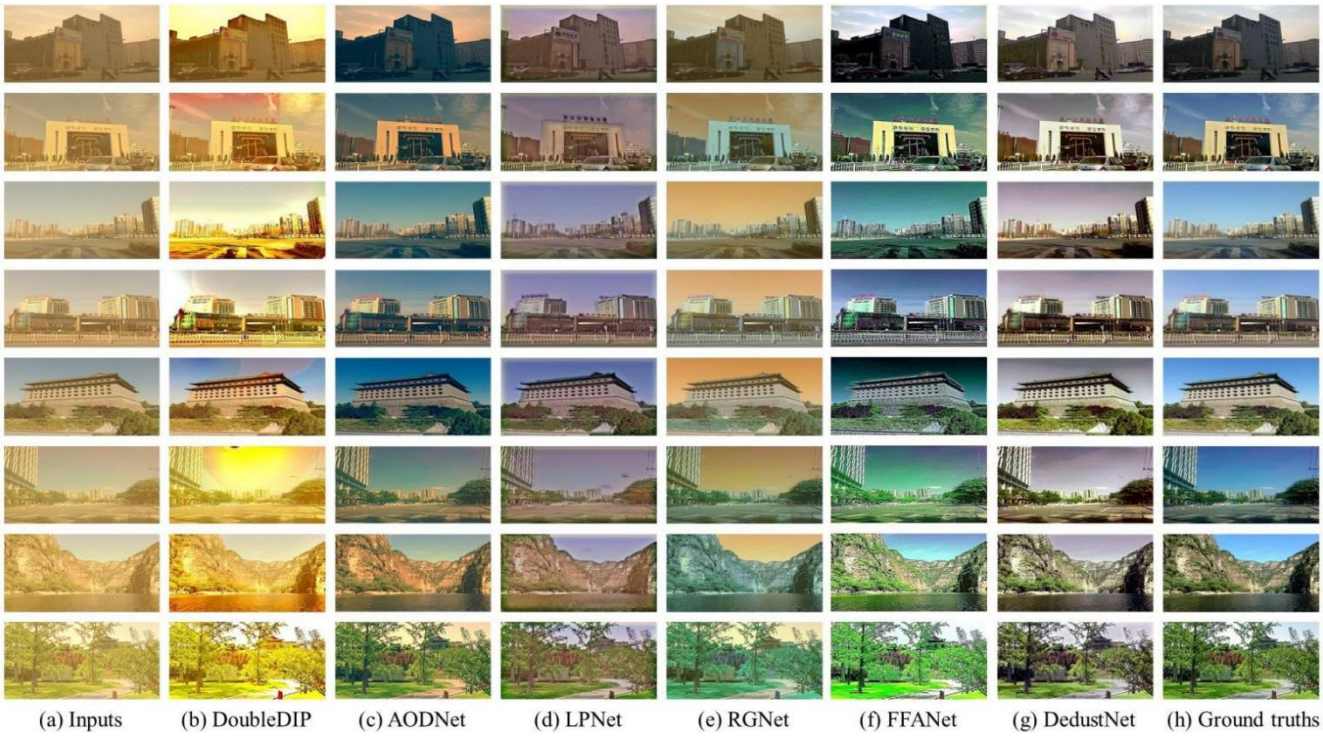

Figure 6. Examples of dedusted results on synthetic dusty images from HTS.

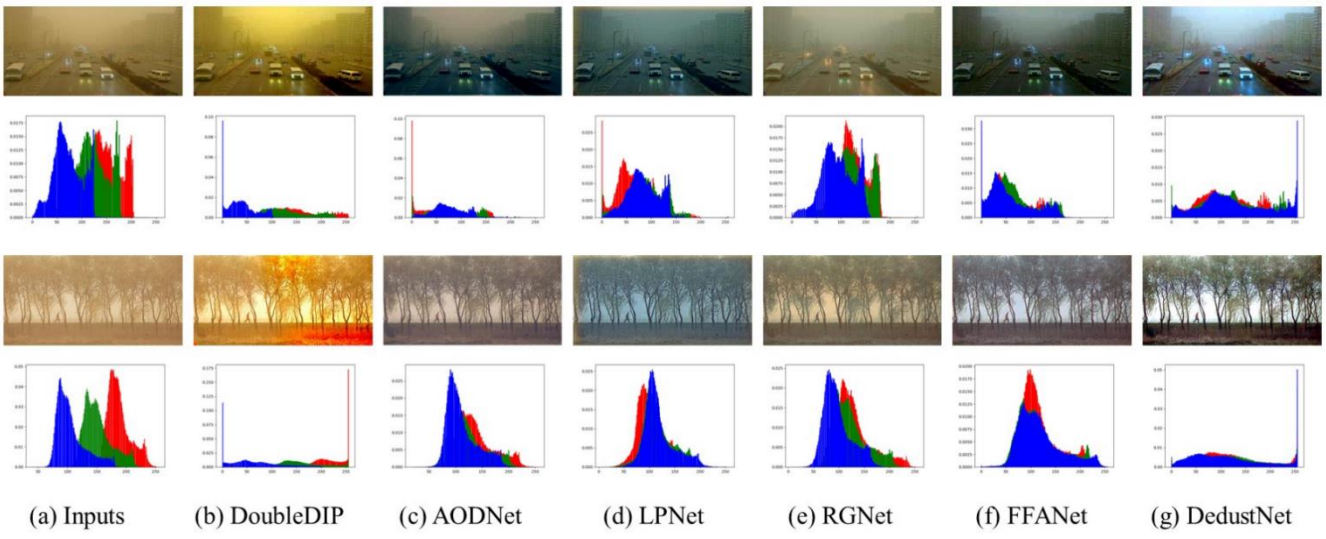

Figure 7. Examples of dedusted results on synthetic dusty images from CTS and ITS respectively.

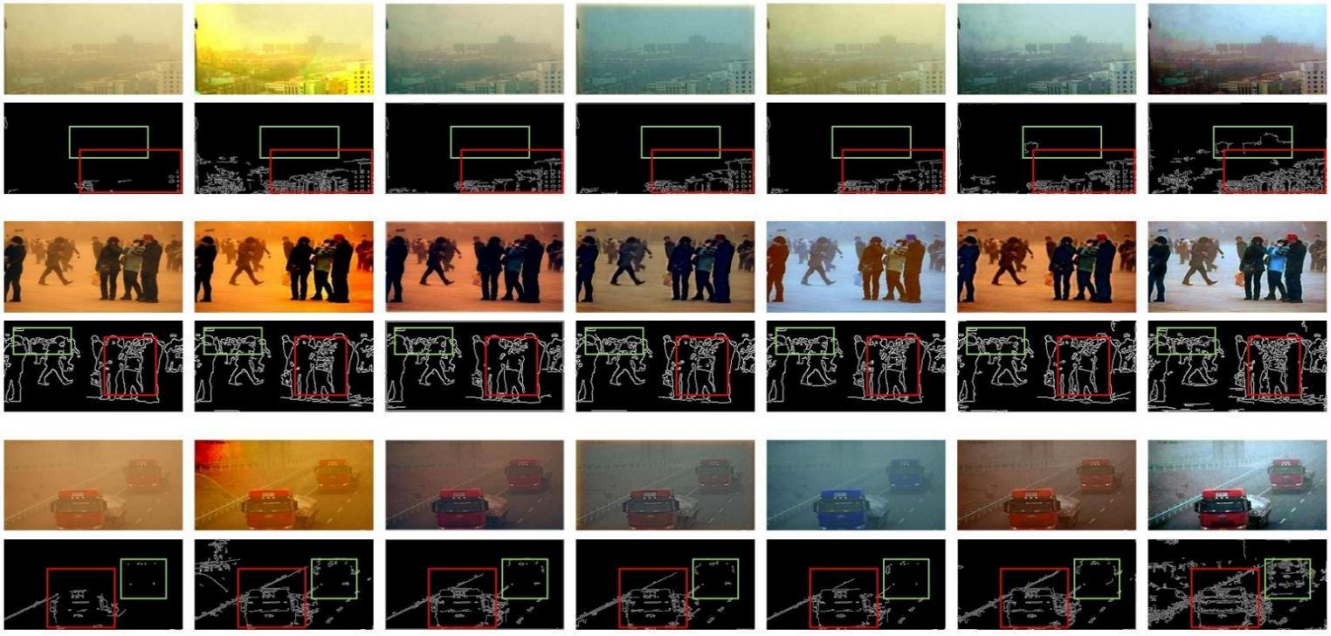

Figure 8. Image edge information extracted from dedusted results obtained by different methods.

Table 4. Comparison of average per-image running time (second) on synthetic images in RSIDR.

Methods	DoubleDIP	AODNet	LPNet	RGNet	FFANet	Ours
Time	180.45	**0.0773**	0.3908	3.0027	1.6167	0.2789

References

[1] C. Wang, A. Grau, E. Guerra, Z. Shen, J. Hu, and H. Fan, "Semi-supervised wildfire smoke detection based on smoke-aware consistency," *Frontiers in plant science*, vol. 13, p. 980425, 2022.
[2] C. Shen, J. Hu, C. Wang, and D. Li, "Lfnet: Lightweight fire smoke detection for uncertain surveillance environment," in *2020 6th Inter-national Conference on Big Data and Information Analytics (BigDIA)*. IEEE, 2020, pp. 11-17.
[3]X. Zhou, Z. Li, H. Xie, T. Feng, Y. Lu, C. Wang, and R. Chen, "Leuko-cyte image segmentation based on adaptive histogram thresholding and contour detection," *Current bioinformatics*, vol. 15, no. 3, pp. 187-195, 2020.
[4] T. Feng, C. Wang, X. Chen, H. Fan, K. Zeng, and Z. Li, "Urnet: A u-net based residual network for image dehazing," *Applied Soft Computing*, vol. 102, p. 106884, 2021.
[5] C. Wang, Z. Li, J. Wu, H. Fan, G. Xiao, and H. Zhang, "Deep residual haze network for image dehazing and deraining," *IEEE Access*, vol. 8, pp. 9488-9500, 2020.
[6] T. Feng, Z. Li, C. Wang, X. Chen, and J. Wu, "Image dehazing network based on dilated convolution feature extraction," *in 2019 12th International Congress on Image and Signal Processing, BioMedical Engineering and Informatics (CISP-BMEI)*. IEEE, 2019, pp. 1-5.
[7] J. Yan, Y. Wang, H. Fan, J. Huang, A. Grau, and C. Wang, "Lepf-net: Light enhancement pixel fusion network for underwater image enhancement," *Journal of Marine Science and Engineering*, vol. 11, no. 6, p. 1195, 2023.
[8] Z. Chen, C. Wang, F. Zhang, L. Zhang, A. Grau, and E. Guerra, "All-in-one aerial image enhancement network for forest scenes," *Frontiers in plant science*, vol. 14, p. 1154176, 2023.
[9] W. Fang, C. Wang, Z. Li, A. Grau, T. Lai, and J. Chen, "Taenet: transencoder-based all-in-one image enhancement with depth aware-ness," *Applied Intelligence*, pp. 1-22, 2024.
[10] X. Zhou, C. Wang, Z. Li, and F. Zhang, "Adaptive histogram thresholding-based leukocyte image segmentation," in *Advances in Intel-ligent Information Hiding and Multimedia Signal Processing: Proceed-ings of the 15th International Conference on IIH-MSP in conjunction with the 12th International Conference on FITAT, July 18-20, Jilin, China, Volume 2*. Springer, 2020, pp. 451-459.
[11] C. Wang, H. Zhang, Z. Li, X. Zhou, Y. Cheng, and R. Chen, "White blood cell image segmentation based on color component combination and contour fitting," *Current Bioinformatics*, vol. 15, no. 5, pp. 463-471, 2020.

[12] X. Zhou, Z. Li, and C. Wang, "Color space volume and superpixel based leukocyte image segmentation," in *2019 10th International Conference on Information Technology in Medicine and Education (ITME)*. IEEE, 2019, pp. 84-88.
[13] M. Zhong, Z. Li, C. Wang, J. Huang, W. Zhao, and H. Fan, "Quality assessment of electrocardiogram signals using contrastive learning," in *2023 13th International Conference on Information Technology in Medicine and Education (ITME)*. IEEE, 2023, pp. 323-328.
[14] H. Zhang, C. Wang, X. Li, B. Sun, and D. Jiang, "Design and imple-mentation of an infrared radiant source for humidity testing," *Sensors*, vol. 18, no. 9, p. 3088, 2018.
[15] F. Zhang and C. Wang, "Msgan: generative adversarial networks for image seasonal style transfer," *IEEE Access*, vol. 8, pp. 104 830-104 840, 2020.
[16] X. Meng, J. Huang, Z. Li, C. Wang, S. Teng, and A. Grau, "Dedustgan: Unpaired learning for image dedusting based on retinex with gans," *Expert Systems with Applications*, vol. 243, p. 122844, 2024.
[17] A. Fu, J. Ma, C. Wang, C. Zhou, Z. Li, and S. Teng, "Traditional chinese medicine health status identification with graph attention network," in *International Conference on Machine Learning for Cyber Security*. Springer, 2022, pp. 1-14.
[18] J. Huang, H. Xu, G. Liu, C. Wang, Z. Hu, and Z. Li, "Sidnet: a single image dedusting network with color cast correction," *Signal Processing*, vol. 199, p. 108612, 2022.
[19] C. Godard, O. Mac Aodha, M. Firman, and G. J. Brostow, "Digging into self-supervised monocular depth estimation," in *Proceedings of the IEEE/CVF International Conference on Computer Vision*, 2019, pp. 3828-3838.
[20] M. Cordts, M. Omran, S. Ramos, T. Scharwächter, M. Enzweiler, R. Benenson, U. Franke, S. Roth, and B. Schiele, "The cityscapes dataset," in *CVPR Workshop on the Future of Datasets in Vision*, vol. 2, 2015.
[21] N. Silberman, D. Hoiem, P. Kohli, and R. Fergus, "Indoor segmentation and support inference from rgbd images," in *European conference on computer vision*. Springer, 2012, pp. 746-760.
[22] L. Liu, B. Liu, H. Huang, and A. C. Bovik, "No-reference image quality assessment based on spatial and spectral entropies," *Signal processing: Image communication*, vol. 29, no. 8, pp. 856-863, 2014.
[23] Y. Gandelsman, A. Shocher, and M. Irani, "" double-dip": Unsupervised image decomposition via coupled deep-image-priors," in *Proceedings of the IEEE/CVF Conference on Computer Vision and Pattern Recognition*, 2019, pp. 11 026-11 035.
[24] B. Li, X. Peng, Z. Wang, J. Xu, and D. Feng, "Aod-net: All-in-one dehazing network," in *Proceedings of the IEEE international conference on computer vision*, 2017, pp. 4770-4778.
[25] X. Fu, B. Liang, Y. Huang, X. Ding and P. John, "Lightweight pyramid networks for image deraining," in *IEEE transactions on neural networks and learning systems*, vol. 31, no. 6, pp. 1794-1807, 2019.
[26] Z. Fan, H. Wu, X. Fu, Y. Huang, and X. Ding, "Residual-guide network for single image deraining," in *Proceedings of the 26th ACM international conference on Multimedia*, 2018, pp. 1751-1759.
[27] X. Qin, Z. Wang, Y. Bai, X. Xie, and H. Jia, "Ffa-net: Feature fusion attention network for single image dehazing," in *Proceedings of the AAAI Conference on Artificial Intelligence*, vol. 34, no. 07, 2020, pp. 11 908-11 915.